Journal of Great Lakes Research 45 (2019) 508–521

Contents lists available at ScienceDirect

Journal of Great Lakes Research

journal homepage: www.elsevier.com/locate/jglr

Satellite monitoring of harmful algal blooms in the Western Basin of Lake Erie: A 20-year time-series

Michael J. Sayers [a,*], Amanda G. Grimm [a], Robert A. Shuchman [a], Karl R. Bosse [a], Gary L. Fahnenstiel [a], Steven A. Ruberg [b], George A. Leshkevich [b]

[a] Michigan Tech Research Institute, Michigan Technological University, 3600 Green Court, Suite 100, Ann Arbor, MI 48105, USA
[b] Great Lakes Environmental Research Laboratory, National Oceanic and Atmospheric Administration, 4840 S. State Road, Ann Arbor, MI 48108, USA

ARTICLE INFO

Article history:
Received 15 May 2018
Accepted 14 December 2018
Available online 20 January 2019

Communicated by Joseph Ortiz

Keywords:
Lake Erie
Harmful algal blooms
Satellite
Cyanobacteria
Time series
Remote sensing

ABSTRACT

Blooms of harmful cyanobacteria (cyanoHABs) have occurred on an annual basis in western Lake Erie for more than a decade. Previously, we developed and validated an algorithm to map the extent of the submerged and surface scum components of cyanoHABs using MODIS ocean-color satellite data. The algorithm maps submerged cyanoHABs by identifying high chlorophyll concentrations (>18 mg/m^3) combined with water temperature >20 °C, while cyanoHABs surface scums are mapped using near-infrared reflectance values. Here, we adapted this algorithm for the SeaWiFS sensor to map the annual areal extents of cyanoHABs in the Western Basin of Lake Erie for the 20-year period from 1998 to 2017. The resulting classified maps were validated by comparison with historical *in situ* measurements, exhibiting good agreement (81% accuracy). Trends in the annual mean and maximum total submerged and surface scum extents demonstrated significant positive increases from 1998 to 2017. There was also an apparent 76% increase in year-to-year variability of mean annual extent between the 1998–2010 and 2011–2017 periods. The 1998–2017 time-series was also compared with several different river discharge nutrient loading metrics to assess the ability to predict annual cyanoHAB extents. The prediction models displayed significant relationships between spring discharge and cyanoHAB area; however, substantial variance remained unexplained due in part to the presence of very large blooms occurring in 2013 and 2015. This new multi-sensor time-series and associated statistics extend the current understanding of the extent, location, duration, and temporal patterns of cyanoHABs in western Lake Erie.

Introduction

Cyanobacteria blooms are recurring events within biologically-productive waters of the Great Lakes and notably the Western Basin of Lake Erie (WBLE) (Vanderploeg et al., 2001; Bridgeman et al., 2013). Harmful algal blooms dominated by the cyanobacterium *Microcystis* (here termed cyanoHABs) have affected recreation, charter fishing, and tourism in the Great Lakes and placed drinking water supplies for millions of consumers at risk. A cyanoHAB in western Lake Erie in 2014 resulted in a three-day tap water ban for approximately half a million customers in Toledo, Ohio (Wynne and Stumpf, 2015). *Microcystis* produces microcystin, a hepatotoxin that can cause gastroenteritis, liver damage and, in extreme cases, more serious illness and even death (Rinta-Kanto et al., 2005). *Microcystis* blooms have occurred on an annual basis in the Western Basin of Lake Erie for more than a decade (Budd et al., 2001; Rinta-Kanto et al., 2005; Stumpf et al., 2012; Steffen et al., 2014).

Due to their temporal and spatial variability ("patchiness"), cyanoHABs are extremely difficult to monitor using buoy- or ship-based sampling (Kutser, 2004). Their concentrations can vary by multiple orders of magnitude over the distance of a few meters. Satellite remote sensing provides the potential for long-term synoptic monitoring of cyanoHAB events which can improve our understanding of these phenomena to allow for the development of approaches that reduce their incidence over the longer term.

Satellite remote sensing has been extensively used to map cyanobacteria bloom dynamics in many areas throughout the world with great success (Pettersson and Pozdnyakov, 2012). Several early electro-optical (EO) satellite platforms, including Landsat 2 and the Coastal Zone Color Scanner (CZCS), proved useful to detect significant accumulations of cyanobacteria blooms in the Baltic Sea (Ulbricht, 1983) and southwestern tropical Pacific Ocean (Dupouy et al., 1988). Additionally, Advanced Very High Resolution Radiometer (AVHRR) thermal imagery was used to relate local increases in sea surface temperature (SST) to surface accumulations of cyanobacteria in the Baltic Sea (Kahru et al., 1993). Since the publication of these early studies, research using satellite remote sensing to map cyanobacteria has

* Corresponding author.
E-mail address: mjsayers@mtu.edu (M.J. Sayers).

https://doi.org/10.1016/j.jglr.2019.01.005

expanded in the literature (Cullen et al., 1997) with work including many areas throughout the world, with notable examples in the Baltic Sea (Kahru, 1997; Kahru et al., 2000, 2007; Kahru and Elmgren, 2014; Miller et al., 2006; Reinart and Kutser, 2006), Lake Taihu (Duan et al., 2009, 2012; Hu et al., 2010; Huang et al., 2014), and South African Lakes (Matthews et al., 2010, 2012; Matthews, 2014; Matthews and Bernard, 2015; Oberholster and Botha, 2010).

Remote sensing algorithms have progressed from the early radiance threshold approaches to more robust empirical and semi-analytical methods as observing system capabilities have increased and better understanding of the underlying cyanobacteria optical properties were achieved (Mishra et al., 2017). Robust algorithms to retrieve chlorophyll-*a* concentrations of cyanobacteria blooms have been developed and adapted for many different freshwater systems to track spatio-temporal dynamics (Gons, 1999; Mishra and Mishra, 2012; Li et al., 2013). In parallel, algorithms were also developed (Dekker, 1993; Schalles and Yacobi, 2000; Simis et al., 2005, 2007; Li et al., 2015) to estimate the presence of phycocyanin, a phycobilin pigment unique to cyanobacteria, allowing for better determination of bloom composition. However, while many cyanobacteria remote sensing algorithms have been developed over the past 30 years, regional tuning or parametrization is often required to adapt to the local scale cyanobacteria/phytoplankton dynamics of individual systems.

In some areas within the Great Lakes basin, cyanoHABs have been shown to occur in highly productive waters that are relatively shallow, warm, and protected from persistent offshore winds (Ho and Michalak, 2015; Watson et al., 2016). These productive waters are optically complex with the color of the water being determined by the concentrations of three color-producing agents (CPAs): chlorophyll (CHL), colored dissolved organic matter (CDOM), and suspended mineral (SM) particles (Jerlov, 1976; Bukata et al., 1995). Traditional marine water color retrieval algorithms developed for the open ocean, whose optical properties are dominated by phytoplankton absorption and scattering alone, typically fail in optically complex waters (Budd and Warrington, 2004; Witter et al., 2009; Ali et al., 2014). Additionally, traditional marine atmospheric correction procedures often yield erroneous water leaving radiance values in optically complex water further reducing the ability of traditional ocean-color retrieval algorithms to produce reliable results (Dash et al., 2012).

Several methods have been developed and adapted to identify Great Lakes cyanoHABs based on algorithms that relate spectral reflectance values in ocean-color satellite imagery to *in situ* water measurements (*e.g.*, Vincent et al., 2004; Becker et al., 2009; Wynne et al., 2010; Stumpf et al., 2012; Sayers et al., 2016). Of these, the most commonly applied approach has been the cyanobacteria index (CI) developed by Wynne et al. (2008) based on the Fluorescence Line Height (FLH) algorithm (Abbott and Letelier, 1999). Stumpf et al. (2012) used this approach to quantify cyanoHABs in western Lake Erie from 2002 to 2011 and relate the annual bloom extent to river discharge. More recently, Sayers et al. (2016) generated cyanoHAB extent maps using a combination of two modified remote sensing approaches using the MODIS Aqua sensor (MCH and SSI, see Methods section). Here, we adapt the MCH and SSI approach to cyanoHAB mapping for the SeaWiFS sensor to extend the available time series of ocean-color cyanoHAB estimates for western Lake Erie from 1998 to 2017.

Because of the limited time frame for which cyanoHAB maps are available from the MODIS Aqua and MERIS ocean color satellites (now 16 years, 2002–2017), the ability to empirically model the various drivers of annual bloom size and spatial distribution has been limited (Obenour et al., 2014). Ho et al. (2017) recently explored extending the MODIS/MERIS ocean-color time series by combining the Wynne/Stumpf CI with a Landsat-based algorithm. They found good coherence between the Landsat product and CI with respect to the macro-scale characteristics of annual peak bloom area. However, Landsat's utility for monitoring the temporal variations of the western Erie cyanoHAB within a season are seriously limited by the satellite's 16-day revisit cycle and by the high annual mean cloud cover in the Great Lakes (Ju and Roy, 2008), resulting in few cloud-free Landsat scenes of western Lake Erie collected per season. The combined SeaWiFS/MODIS time series of cyanoHAB extent presented here can both serve as additional years of evaluation data for Landsat algorithms and help improve the knowledge of Lake Erie cyanoHAB spatial heterogeneities and finer-scale temporal variability needed to gain a mechanistic understanding of the dynamics of cyanoHAB development and distribution.

In this study, we investigate the coherence of SeaWiFS and MODIS-based cyanoHAB products in a combined time series of hindcast cyanoHAB extent for western Lake Erie. A series of empirically-based adjustments were made to reconcile the cyanoHAB classification differences between the two platforms observed for overlapping images. The aims of this study are to: (i) document the adaptation of the MCH/SSI approach for cyanoHAB mapping to the SeaWiFS satellite; (ii) evaluate the SeaWiFS-derived cyanoHAB maps through comparison with *in situ* data and with MODIS-derived maps for overlapping dates; and (iii) revisit the Sayers et al. (2016) discussion of the local factors driving annual cyanoHAB dynamics in light of this longer time series.

Methods

Satellite imagery

SeaWiFS and MODIS uncalibrated Level 1A imagery was downloaded from the NASA OceanColor data portal (https://oceancolor.gsfc.nasa.gov). Level 1A data were processed to Level 2 (georeferenced with atmospheric and radiometric calibrations) using NASA SeaDAS software. A fixed model pair aerosol correction and custom cloud masking approach was applied to the images to ensure that the high NIR reflectance values of surface scum pixels were not interpreted as atmospheric contamination (Sayers et al., 2016). Additionally, Sayers et al. (2016) reported that the fixed-model pair aerosol selection approach resulted in more consistent and accurate remote sensing reflectance values than the standard oceanic black pixel assumption method during significant cyanoHAB events in western Lake Erie.

Each cloud-free or mostly (>80%) cloud-free image of the Western Basin of Lake Erie (Fig. 1) collected by SeaWiFS between mid-1997 and 2007 or by MODIS Aqua between mid-2002 and 2017 at times when the water temperature in the Western Basin was above 20 °C—the minimum temperature favorable to cyanoHAB development (Sayers et al., 2016)—was downloaded. The 20 °C threshold was developed to reduce the number of false cyanoHAB identifications in cooler water (<20 °C) periods when blooms of other phytoplankton, particularly diatoms, can occur (Sayers et al., 2016). When an image with partial cloud cover or other interference was collected within 3 days of a better-quality image, only the better scene was retained in the image set. The dates when the temperature exceeded and then fell below the 20 °C threshold for each year were determined using the AVHRR (pre-2002) and MODIS (2002–2017) Sea Surface Temperature (SST) product. The satellite-observed water temperatures were verified with buoy measurements from the National Data Buoy Center (NDBC) when available (https://www.ndbc.noaa.gov/).

Bio-optical models

The hybrid bio-optical and vegetation index method of cyanoHAB mapping described in Sayers et al. (2016) was applied to MODIS Aqua imagery from 2014 through 2017 to extend the 2002–2013 time series presented in that paper. Briefly, the first approach (modified CPA-A HABs, or MCH) was a modification of the CPA Algorithm (CPA-A), a semi-analytical bio-optical chlorophyll-*a* retrieval algorithm which simultaneously optimizes estimated concentrations for all three CPAs using a hydro-optical model derived from extensive *in situ* measurements collected in western Lake Erie (Shuchman et al., 2006, 2013).

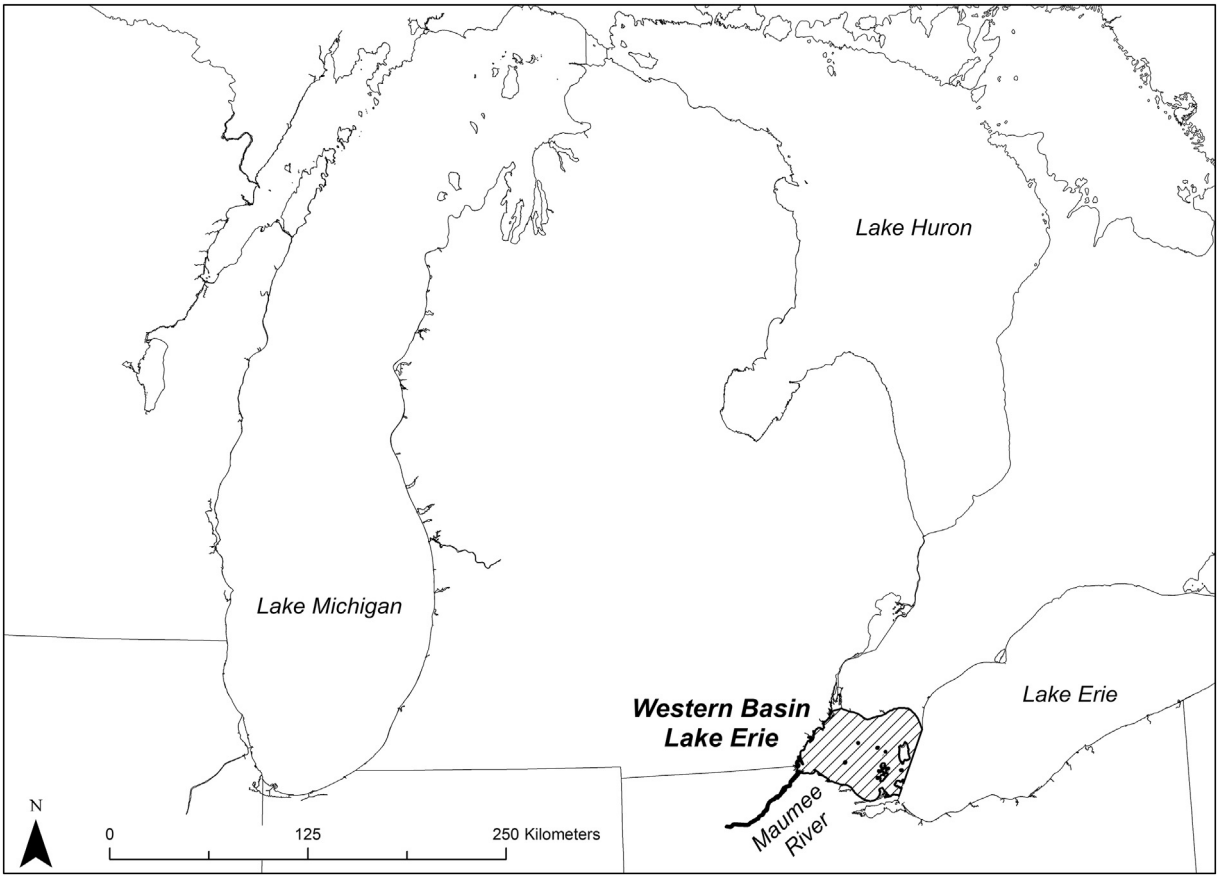

Fig. 1. The western Lake Erie study area is defined by the hatched area. The Maumee River is also shown as bold black line entering the basin.

For cyanoHAB detection, the CPA-A is enhanced with empirical relationships between chlorophyll-*a* and environmental variables and leveraged using the observed linear relationship between surface chlorophyll-*a* and phycocyanin pigment concentrations in western Lake Erie to estimate water column cyanoHABs. A threshold value of 18 mg m^{-3} of chlorophyll-*a* was used to classify pixels as cyanoHAB based on a segmented regression analysis (Sayers et al., 2016). Briefly, using *in situ* data from three eutrophic basins in the Great Lakes (Green Bay, Saginaw Bay, and western Lake Erie), Sayers et al. (2016) established a significant linear relationship between chlorophyll-*a* and phycocyanin when chlorophyll-*a* was >18 mg m^{-3}. The authors noted there was little to no abundance of phycocyanin for chlorophyll-*a* concentrations < 18 mg m^{-3}. MODIS-estimated water temperature was also used to distinguish between blooms of cyanobacteria (>20 °C) and other phytoplankton such as diatoms and green algae (<20 °C) (Sayers et al., 2016).

Historically, cyanoHAB mapping algorithms in the Great Lakes have not differentiated surface algal scums from sub-surface cyanobacteria in the water column (Sayers et al., 2016). *In situ* monitoring in Lake Erie has consistently indicated that the floating algae mats, or surface scums, that sometimes form during cyanoHAB events in Lake Erie contain extremely high concentrations of *Microcystis* which has the potential to affect public health. Thus, the second approach described in Sayers et al. (2016), the surface scum index (SSI, Eq. (1)) used a band ratio index to detect cyanoHAB surface scums:

$$SSI = \left(\frac{(NIR)-(VIS)}{(NIR)+(VIS)}\right) > 0 \quad (1)$$

where NIR represents spectral reflectance in a near-infrared satellite band and VIS represents reflectance in a visible-range band, usually red. Positive values in known water pixels were classified as surface cyanobacteria scum based on the high reflectance of algae scum at NIR wavelengths relative to low red reflectance controlled by chlorophyll (and other pigments) absorption. Other researchers have used similar approaches to successfully detect surface algae in other freshwater regions throughout the world using sensor specific methodology (Peng et al., 2008; Hu, 2009; Hu et al., 2010; Matthews et al., 2012). It should be noted that there is no procedure for differentiating cyanobacteria scum from other floating macrophytes either living or not living. However, because of the relatively large pixel size (250 m for MODIS) it would require a significant bed or wrack of floating macrophytes to trigger a positive SSI value. MODIS bands 9–13 (band centers: 443, 488, 531, 547, 667 nm; 1 km resolution) were used in the MCH, and MODIS bands 1 and 2 (645 and 858 nm, respectively; 250 m resolution) were used in the SSI.

Satellite sensor inter-calibration

To generate cyanoHAB maps from SeaWiFS imagery, the MCH/SSI approach was initially applied with minimal modification, using bands 2–6 (band centers: 443, 490, 510, 555, and 670 nm; 1 km resolution) for the MCH, bands 6 and 8 (670 and 865 nm, respectively; 1 km resolution) to calculate the SSI, and AVHRR SST as the water temperature input. This initial product was compared with the previously validated, MODIS-derived product for a selection of dates from 2002 to 2007 when both sensors collected cloud-free images. Comparing the outputs for the two sensors indicated that scum was initially under-classified in SeaWiFS imagery, a problem that was corrected through a series of empirically-based adjustments.

First, the MODIS-derived SSI product was compared to two SeaWiFS-derived SSI products: the original version, using SeaWiFS band 8 centered at 865 nm as the NIR input to the SSI algorithm, and a second version using band 7 centered at 765 nm. It was determined

that the 765 nm SeaWiFS SSI was more similar to the MODIS product based on Spearman rank correlation of SSI values for matched grid cells. Second, it was observed that the SeaWiFS SSI was systematically lower than MODIS SSI, in part due to the differences in sensor design characteristics (bandwidth, signal-to-noise, *etc.*,) between MODIS Aqua and SeaWiFS. To compensate for these differences and obtain a SeaWiFS SSI product comparable to the MODIS product, the empirical relationship between the SeaWiFS and MODIS SSI products over the overlap period between the two datasets (2002−2010) was used to apply an adjustment factor to the threshold value at which SeaWiFS SSI is classified as scum. Third, these changes to the SeaWiFS SSI created problems with some scum areas being misclassified as clouds; this was corrected with a simple threshold filter using the cumulative reflectance of SeaWiFS visible bands. Fourth, several pixels along the shoreline were consistently flagged as scum, even outside of the cyanoHAB season, due to spatial resolution differences between SeaWiFS and the MODIS-based land mask utilized in the MCH/SSI method. This was resolved by editing the land mask to exclude those pixels, yielding a slightly smaller mapped water surface area. The cumulative effect of these adjustments is illustrated by Fig. 2. Finally, the absorption coefficients included in the hydro-optical model utilized for the CPA-A were also adjusted by comparing the results for MODIS and SeaWiFS for the same dates and applying a vicarious calibration correction.

SeaWiFS product verification

In situ chlorophyll-*a* measurements collected in western Lake Erie during the cyanoHAB season (August–September) between 1997 and 2007 were retrieved from EPA's Great Lakes Environmental Database (GLENDA, http://www.epa.gov/glnpo/monitoring/data_proj/glenda/), from the NOAA Great Lakes Environmental Research Laboratory's International Field Years on Lake Erie (IFYLE) Cruise Database (Hawley et al., 2006; https://www.glerl.noaa.gov/res/projects/ifyle/), and from the University of Toledo's Western Erie cruise database (Bridgeman et al., 2013). *In situ* surface water chlorophyll-*a* concentrations > 18 mg/m^3 when the water temperature was >20 °C were considered to potentially represent a cyanoHAB based on previous analyses (Wynne et al., 2013; Sayers et al., 2016). Because presence of surface scum was not recorded, SSI was not evaluated separately from bloom presence/absence. Table 1 below summarizes the combined GLENDA, IFYLE and UT *in situ* data set used to evaluate the SeaWiFS MCH product. The product was evaluated by comparing each *in situ* observation to the value of the individual SeaWiFS pixel that the observation falls within. Observations were compared to the SeaWiFS image collected closest in time to the observation, up to a maximum of 3 days. It should be acknowledged that a single *in situ* observation may or may not be spatially representative of the water encapsulated within a single satellite pixel, ~1 km in the case of SeaWiFS, however it is difficult to quantify this uncertainty with the available data. A previous study conducted a sensitivity analysis to confirm that using *in situ* observations taken within three days of an image collection for algorithm evaluation purposes does not decrease estimated algorithm accuracy relative to using observations from within 12 h or one day (Ho et al., 2017).

Table 1
Numbers of available *in situ* water quality samples measured in the western basin of Lake Erie within 3 days of a cloud-free SeaWiFS image collection during a cyanoHAB season between 1998 and 2007. There were no valid matchups in 2000 or 2001.

Year	1998	1999	2002	2003	2004	2005	2006	2007	Total
HAB	0	0	8	12	15	4	4	4	47
No HAB	6	12	11	16	11	20	11	9	96
Total	6	12	19	28	26	24	15	13	143

SeaWiFS and MODIS product inter-comparison

The SeaWiFS- and MODIS Aqua-derived cyanoHAB products were compared at both the pixel and basin scales. First, the similarity of the classified map products (based on a simple matching coefficient) was calculated for 89 pairs of images collected on the same day between 2002 and 2007 to quantify the similarity of bloom identification at specific locations between sensors. The time difference between the two image collections ranged from 11 s to 1 h 46 min with a mean of 30 min. Pixels flagged as cloud cover were excluded from the comparison. Second, bloom areas were compared across this same set of date-matched image pairs to evaluate the similarity of mapped bloom magnitudes between sensors. Coefficients of determination and root mean squared errors from weighted least squares regression between the SeaWiFS- and MODIS-estimated annual mean surface scum and total bloom areas were used to assess map similarity. Regression weights were based on the number of pixels flagged as clouds in the SeaWiFS image to account for the increase in uncertainty with cloud cover. Weights were calculated as $w_i = 1 - (c/a)$, where w_i is the weight applied for the ith date-matched image pair, c is the cloud-covered area in the SeaWiFS image (km^2) and a is the total mapped area in the Western Basin (2984 km^2). Finally, a similar regression was performed using only the annual maximum surface scum and total bloom areas for each sensor.

Time-series analysis

After a quantitative comparison between the sensors' derived products was completed, their data was combined to form a 20-year time series, extending the 12-year record reported by Sayers et al. (2016). The SeaWiFS data was used from 1998 to 2001 and the MODIS Aqua data was used from 2002 to 2017. Annual mean cyanoHAB and scum extent were determined by taking the mean extent of high chlorophyll-*a* (based on the MCH method) and scum (based on the SSI method),

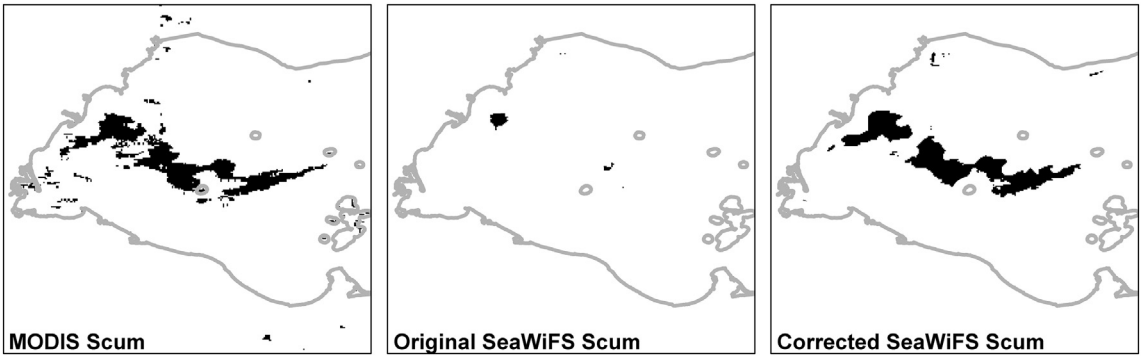

Fig. 2. Comparison of SSI-based scum classification results from MODIS (left panel), the initial SeaWiFS result (center panel), and the corrected SeaWiFS result (right panel) for June 22, 2003. Black cells represent positive surface scum observations.

respectively, in all cloud-free images within the 20 degree surface temperature window. Annual maximum extents for each product were determined by taking the mean of the largest three extents for each year. Seasonal trends were studied by breaking each year into 20 8-day windows ranging from mid-May to mid-October and finding the mean extents within each window.

In WBLE, increases in cyanoHABs had previously been linked to nutrient loading and climate change (Stumpf et al., 2012; Michalak et al., 2013). Using the MODIS Aqua cyanoHAB algorithm (described in the Bio-optical model section) for imagery collected from 2002 to 2013, Sayers et al. (2016) found that mean annual MCH and SSI extents were significantly related to mean spring (March–June) discharge. This analysis extended those comparisons to the longer 20-year SeaWiFS/MODIS time series. Two discharge metrics were used in determining this relationship. The first method was to use mean annual spring (March–June) discharge (Q), consistent with historic discharge modeling (Stumpf et al., 2012; Sayers et al., 2016). The second method was to use half-weighted March–June discharge and add in fully weighted July discharge only when the mean June water temperatures were found to be above 20 degrees Celsius. This method will be referred to as weighted discharge, or wQ. This discharge formulation comes from Stumpf et al. (2016) and was found to more accurately predict bloom severity. Sayers et al. found a significant linear relationship between discharge and MCH and a significant cubic relationship between discharge and SSI (Sayers et al., 2016). Stumpf et al. found that discharge and CI were best modeled with an exponential model (Stumpf et al., 2012, 2016).

Mean daily discharge from the Maumee River was obtained from USGS observations (http://waterdata.usgs.gov/nwis/) using station 04193500 at Waterville, Ohio. Monthly discharge data were derived as the sum of the daily discharges. June water temperature was determined based on satellite imagery, averaging the surface water temperatures of the southern section of the western basin as defined in Stumpf et al. (2016) - south of the north end of Pelee Island (41.914 N) and west of Marblehead (82.741 W). Monthly SST data from 1998 to 2002 were generated from daily AVHRR data composited using the GLSEA model (Schwab et al., 1999). For 2003–2017, MODIS Aqua Level 3 Monthly 4 μ SST (downloaded from the NASA OceanColor data portal) was used. Regression analyses between each discharge metric and mean annual cyanoHAB and scum extents were performed in R to determine which regression model is most explanatory and whether either discharge metric is an effective indicator of cyanoHAB extent.

Results

The Julian days of cloud free images for SeaWiFS (1998–2001) and MODIS (2002–2017) are shown in Fig. 3 as black dots. The date at which the water temperature exceeded and fell below 20 °C are identified as an X symbol on each line, with the left most and right most X symbols representing the onset and end of 20 degrees respectively. In some years (*e.g.* 2007, 2016) there are several images just outside of the satellite observed 20 degree water temperature period. These dates were included as buoy temperature measurements were still above 20 degrees. Cloud free images are generally well distributed throughout the cyanoHAB season, however, there are several periods of prolonged cloud cover (*e.g.* September 2006, July 2013) that prohibited the estimation of cyanoHAB extents in these periods. Typically, there were fewer quality images obtained for the SeaWiFS period partially due to clouds as well as imperfect atmospheric correction.

The SeaWiFS-derived cyanoHAB mapping products agreed well with the *in situ* observations (Table 2). CyanoHAB events were defined as remote sensing derived pixel values and *in situ* measurements with chlorophyll concentration > 18 mg/m^3. The overall accuracy of 81% is slightly lower than that obtained for the MODIS Aqua product (87% for MCH;

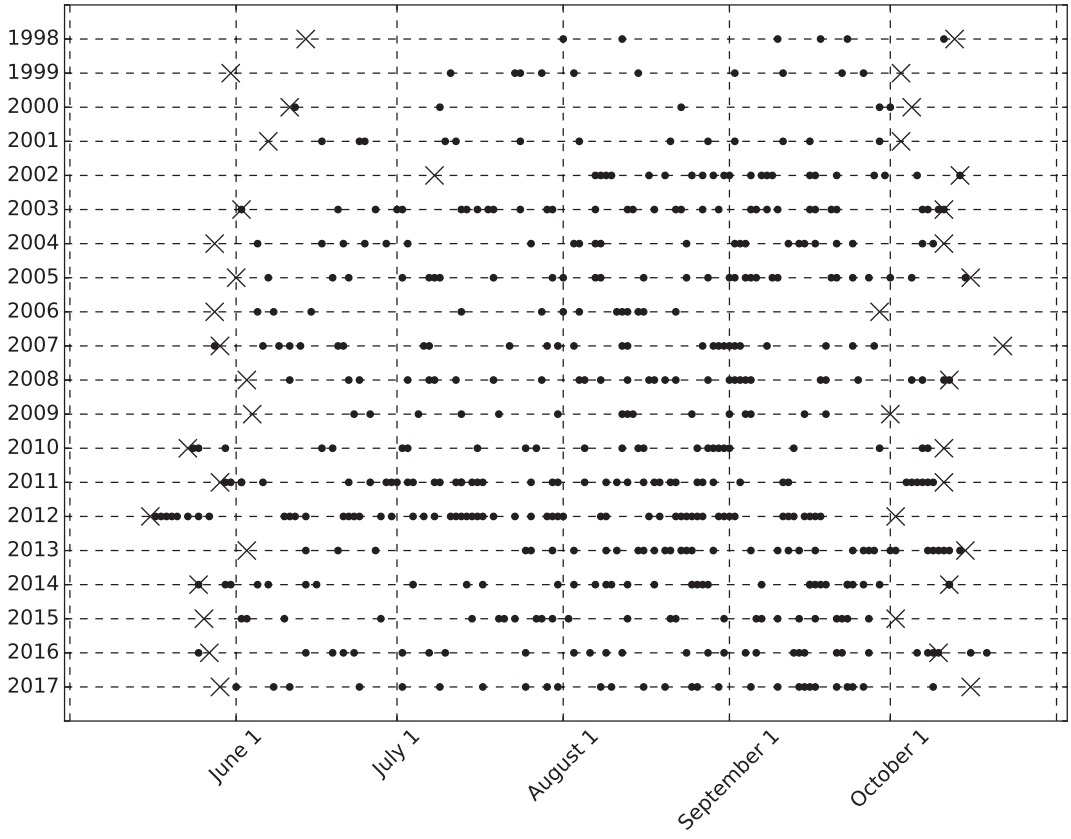

Fig. 3. Cloud free images (black dots) used to generate combined 20 year time series data set. SeaWiFS images were used from 1998 to 2001 and MODIS from 2002 to 2017. Also shown (black X) are the 20 degree onset and offset dates established from satellite surface water temperature observations.

Table 2
Classification error matrix for SeaWiFS-derived MCH *vs. in situ* observations. The hybrid algorithm agreed with 116 out of 143 *in situ* observations for an overall accuracy of 81% and Kappa coefficient of 0.57.

		Field truth				
		HAB	No HAB	Total	User's accuracy	Commission error
SeaWiFS	HAB	33	13	46	72%	28%
	No HAB	14	83	97	86%	14%
	Total	47	96			
	Producer's accuracy	70%	86%		Overall accuracy	81%
	Omission error	30%	14%		Kappa	0.57

Sayers et al., 2016). False positive and false negative classifications were equally frequent. Classification accuracy was lower when a cyanoHAB was present (70%) than when absent (86%). Misclassified pixels tended to be located near the edge of a bloom. There was no strong seasonal trend in validation accuracy. This assessment confirms the suitability of SeaWiFS for the MCH approach to cyanoHAB mapping.

At the pixel scale, the average similarity of the 89 date-matched pairs of images was 89% (simple matching coefficient, SMC). There was no significant relationship between SMC and the time difference between MODIS Aqua and SeaWiFS collections (Pearson's $r = -0.12$, $n = 89$, $p = 0.28$). This is in line with expectations given the similar overpass times of SeaWiFS and MODIS Aqua for Lake Erie, and supports the integration of SeaWiFS- and MODIS Aqua-derived cyanoHAB estimates into a single time series.

At the basin scale, the weighted coefficient of determination (wR^2) and the root mean squared error (RMSE) for the weighted linear regressions of the mean basin wide bloom area date-matched pairs ($n = 89$) indicated relatively strong agreement at 0.81 and 297 km^2 respectively. These uncertainty values are similar to those reported by Ho et al. (2017) when comparing Landsat and MERIS cyanoHAB extents. The coefficient of determination (R^2) and RMSE for annual maximum areas ($n = 6$) were 0.74 and 421 km^2, respectively. The annual maximum extent RMSE (421 km^2) between the SeaWiFS and MODIS observations was approximately 14% of the mapped area of the basin (2984 km^2). This result is reasonable considering that the maximum extent observed by each sensor may not have occurred on the same day, for example in 2002 the SeaWiFS maximum extent was observed on August 8th while the MODIS maximum was on August 31st. The discrepancy between sensor observed maxima are partially due to cloud formation between sensor overpasses or suboptimal viewing geometry of one platform relative to the other as well as shoreline effects. While there is no established threshold criteria to evaluate successful multi-sensor ocean color product merger (IOCCG, 2007), the agreement (wR^2) between SeaWiFS and MODIS cyanoHAB merged products identified in this study is similar to those identified for other global ocean color product mergers.

Finally, the SeaWiFS and MODIS Aqua products for the overlapping 2002–2007 years, described in the SeaWiFS and MODIS Product Intercomparison section, were compared based on the annual mean and maximum cyanoHAB areas (Fig. 4, top panel) and surface scum areas (Fig. 4, bottom panel). Trends in mean and maximum annual cyanoHAB area, as derived from the MCH algorithm, were very similar between sensors, with a mean difference of 16% in overlapping years for both metrics. Surface scum area showed more divergence between sensors, with 68% and 64% difference in mean and maximum area, respectively, in overlapping years. The greater disparity in scum areas between sensors is potentially due to the difference in sensor spatial resolution (*i.e.* MODIS is 250 m and SeaWiFS is 1000 m) and the difference in image acquisition time (up to 1 h and 45 min). CyanoHAB surface scums are highly dynamic in their vertical and horizontal distribution forming patches which can quickly advect or mix down into the water column making it problematic to observe similar spatial distributions over short time-scales (Bosse et al., 2019; Lekki et al., 2019). The trends do track fairly well between sensors for these metrics though, with the only clear difference being the maximum scum extent in 2003 where SeaWiFS maximum observed extent was almost two-fold greater than that observed by MODIS.

Combining the SeaWiFS (1998–2001) and MODIS Aqua (2002–2017) data into annual 20-year time series datasets, the mean annual MCH cyanoHAB extent and maximum MCH annual cyanoHAB extent trends along with linear fits and 95% confidence intervals were calculated and are shown in Fig. 5. A significant linear relationship was identified between year and mean annual extent (Fig. 5, left panel, slope = 25.28, $R^2 = 0.34$, $p = 0.007$), however, it is only explaining 34% of the observed variability. The mean annual extent was consistently between 200 and 500 km^2 (representing between 7 and 17% of the WBLE) from 1998 to 2010; however, beginning in 2007, the mean extent displayed an upward trend, peaking in 2015 when the mean cyanoHAB extent exceeded 42% of the basin. Recent years (2010–2017) have shown increased year-to-year variability (Fig. 5, left panel), as indicated by the dramatic up and down cycling of the mean annual extents. The mean percent difference between consecutive annual extent pairs for the 1998–2009 period was 43.9% while the 2010–2017 period was 75.8%, an approximate 76% increase in year-to-year variability between the early (1998–2009) and more recent (2010–2017) periods. The observed increase in inter-annual variability is also evident from the large deviation in mean annual extents from the 95% confidence interval in 2012, 2013, and 2015. Regression model statistics are summarized in Table 3.

The maximum cyanoHAB extent (Fig. 5, right panel) has been consistently and significantly increasing over the 1998–2017 period (slope = 57.7, $R^2 = 0.54$, $p < 0.001$). The maximum observed cyanoHAB extent has increased more than two-fold (linear trend predicted value for 1998 = 802 km^2 and 2017 = 1899 km^2) from 1998 to 2017. Approximately 54% of the observed variability in maximum annual extent is explained by year, which is almost 60% more than for the mean annual extent relationship (Fig. 5, left panel). The annual maximum extent also showed significant variability, with five years (2003, 2005, 2007, 2011, and 2012) falling outside (both above and below) of the 95% confidence interval. Regression model statistics are summarized in Table 3.

Trends in mean and maximum SSI extents were also derived from the combined SeaWiFS and MODIS dataset and are shown in Fig. 6. A significant linear relationship between mean annual SSI extent and year was identified from the time-series data (Fig. 6, left panel, slope = 2.42, $R^2 = 0.39$, $p = 0.003$). While the trend is statistically significant, large year-to-year variability is observed in the 2010–2017 period relative to the earlier years. The maximum scum extent is also increasing significantly (Fig. 6, right panel, slope = 11.29, $R^2 = 0.39$, $p = 0.003$) throughout the 20 year period, however with large inter-annual variability similar to the mean annual scum extent. It is clear from Fig. 6 that large surface scums of cyanoHABs are becoming larger, on average, in the western basin of Lake Erie.

In addition to significant interannual variability, satellite derived cyanoHAB areal extents are highly variable within years (Fig. 7, left panel). Intra-annual cyanoHAB variability (standard deviation of observed bloom areas within each year) varied from 221 km^2 to 633 km^2 with a mean of 442 km^2. Large intra-annual variability was observed for both the early 1998–2010 period and the more recent 2011–2017 period indicating no discernible changes or trends in seasonal variability across the combined 20 year time-series. Some of the observed differences in intra-annual variability between years is the product of a differing number of clear satellite observations (*e.g.* 13 images in 2001 and 25 in 2015) as well as the timing of available cloud-free observations (*e.g.* 2001 had 3 August images and 2015 had 5 August images) while the remaining variability is likely due to seasonal variations in bloom extent.

The seasonal variability of cyanoHAB extent was examined using the combined 20 year time series binned into 8-day composite values. Fig. 7

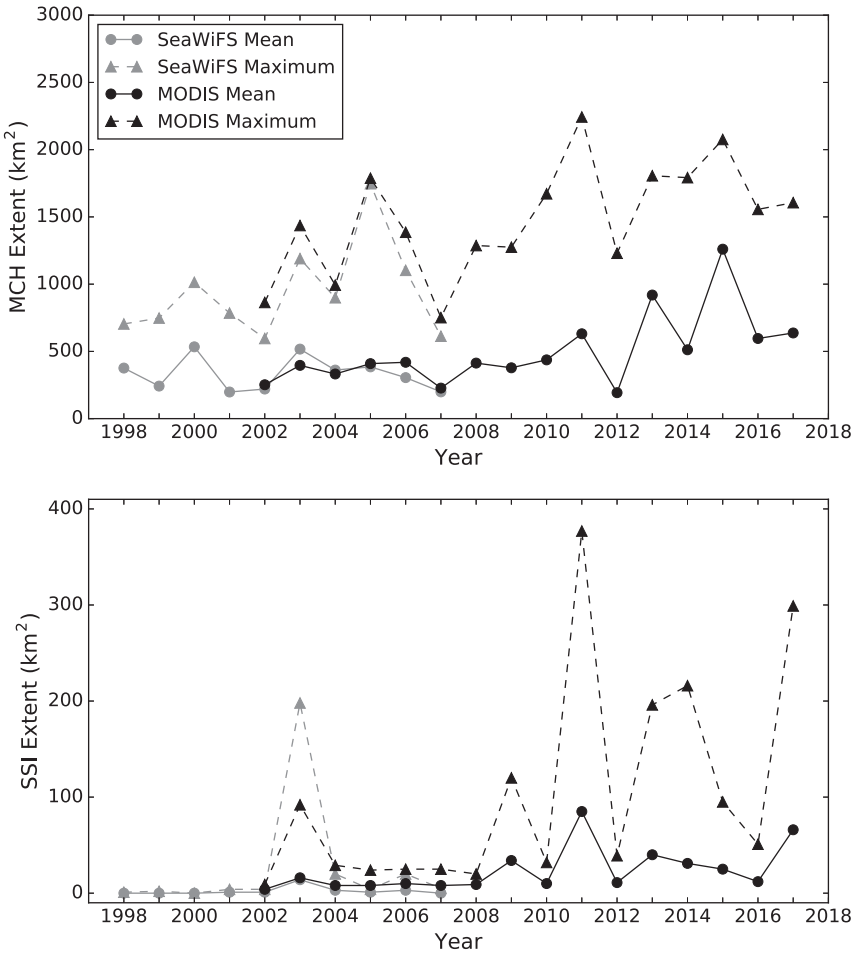

Fig. 4. Comparison of mean and maximum annual cyanoHAB areas based on the MCH (top panel) and surface scum areas based on the SSI (bottom panel) in the Western Basin of Lake Erie for SeaWiFS (1998–2007) and MODIS Aqua (2002–2017).

(right panel) shows the seasonal progression of cyanoHAB extent, derived from the full 20-year data record. This progression shows generally small cyanoHAB extents (<300 km^2) May through June (Day 120–180), followed by a steady increase from mid-July (Day 195) until the cyanoHAB area peaks in mid- to late-September (Day 255–270) and then begins to decline until the end of the season. Variability in extent is evident in each of the 8-day periods with greater variance (453 km^2) occurring once the bloom has initiated (*i.e.* after day 200) relative to pre-initiation variance (185.5 km^2).

The spatial and temporal extent of cyanoHABs during the 20 year period in the western basin can be easily examined with the use of heat maps. A heat map is simply the frequency of occurrence of cyanoHABs

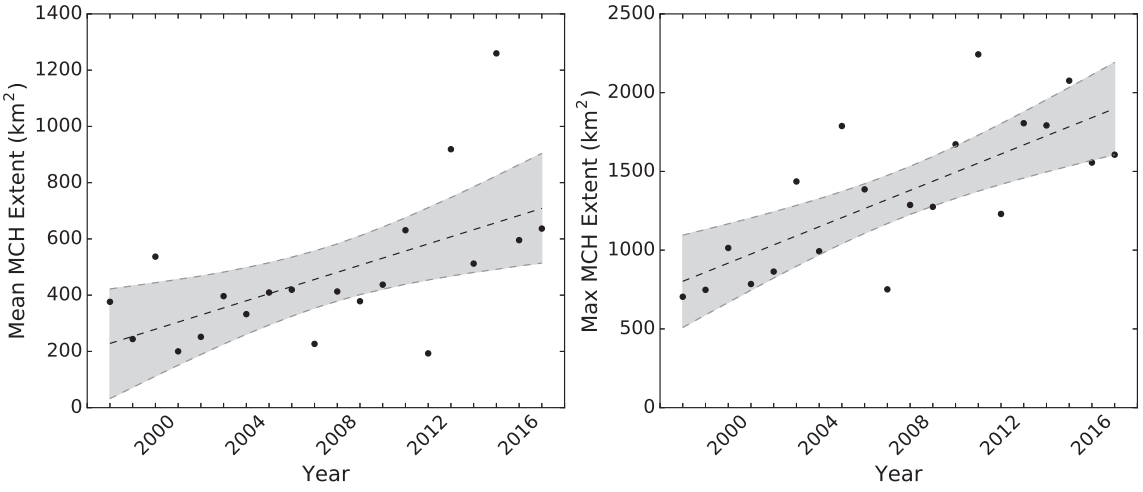

Fig. 5. (left panel) Annual mean cyanoHAB extent (km^2) from the MCH with a linear best fit line (slope = 25.28, $R^2 = 0.34$, $p = 0.007$) and 95% confidence interval shaded in grey and (right panel) annual maximum cyanoHAB extent with a linear best fit line (slope = 57.7, $R^2 = 0.54$, $p < 0.001$) and 95% confidence interval shaded in grey. Points from 1999 to 2001 come from the SeaWiFS sensor; points from 2002 to 2017 come from the MODIS Aqua sensor.

Table 3
Linear regression statistics for the 20-year time series mean and maximum MCH and SSI annual extents.

Extent	Slope	R^2	p-Value
Mean MCH	25.28	0.34	0.007
Maximum MCH	57.7	0.54	<0.001
Mean SSI	2.42	0.39	0.003
Maximum SSI	11.29	0.39	0.003

within each pixel for a given year. Fig. 8 presents annual heat maps for the 1998–2017 period. These annual maps show the increasing extent of cyanoHABs across the basin as well as their spatial patterns which appear to be focused around the mouth of the Maumee River and extend east along the southern edge of the lake while rarely traveling north into the outflow of the Detroit River. The SeaWiFS period (1998–2001) heat maps all show large areas where no cyanoHAB was observed (shown black) within a given year. With the exception of 2007, the large area of cyanoHAB-free water in the western basin has dramatically decreased since 1998, with 2017 exhibiting only 5% percent of the basin as free of cyanoHAB.

Simple heat maps can illustrate the cumulative occurrence of cyanoHABs across the basin over the combined 1998–2017 time series (Fig. 9). The total cyanoHAB heat map (Fig. 9 top panel) is comprised of both water column mixed (MCH) and surface scum (SSI) mapped pixels and represented in weeks of occurrence. The most frequent cyanoHAB occurrences are concentrated in the Michigan and Ohio nearshore areas extending approximately 12–16 km into the basin. Significant occurrences (8–16 weeks) are also observed extending outward to the middle of the basin and amongst the island archipelago to the east. Very few (<4 weeks) cyanoHAB occurrences were detected in the proximity of the Detroit River plume (light and dark blue). The surface scum heat map demonstrates the very limited temporal and spatial extent of these events in the western basin during the 1998–2017 period (Fig. 9 bottom panel). Surface scums were prevalent (>8 days) in the mouth of the Maumee River extending just up the Michigan and Ohio shorelines. There was also significant occurrence of scums near the islands in the middle and eastern end of the basin possibly due to increased accumulation from prevailing winds and underlying currents. Interestingly, there are very few scum occurrences along the southern shore of the basin just north of Sandusky Bay which is in contrast with the total cyanoHAB cumulative distribution that shows wide-spread presence. Finally, very few scum forming blooms are observed in the northern half of the basin in the vicinity of the Detroit River outflow.

In order to better understand drivers controlling mean annual cyanoHAB extent, several previously defined metrics of mean spring discharge for the Maumee River as well as fit types were compared to annual MCH and SSI values for the Western Basin of Lake Erie for 1998–2017 period. In all cases the mean weighted spring discharge metric, *w*Q, (Stumpf et al., 2016) produced more significant relationships with cyanoHAB extent than the mean March–June discharge metric, Q (MCH linear – *w*Q $p = 0.01$, Q $p = 0.019$; MCH exponential - *w*Q $p = 0.002$, Q $p = 0.009$; SSI cubic – *w*Q $p < 0.001$, Q $p = 0.004$, SSI exponential – *w*Q $p = 0.002$, Q $p = 0.011$). The relationships between cyanoHAB extents and *w*Q are shown in Fig. 10. A significant linear relationship was found between *w*Q and MCH ($y = 1.53x + 64.14$, $p = 0.01$, $R^2 = 0.27$; Fig. 10, top left panel). While significant, *w*Q only explains 27% of the variance in mean annual MCH extent due in part to the two extremely large extent years in 2013 and 2015. A significant exponential fit between *w*Q and MCH annual extent was also identified ($y = 165.92 * 10^{0.022X}$, $p = 0.002$, $R^2 = 0.39$; Fig. 10, top right panel). The exponential model is better than the linear model for predicting MCH annual extent, however, it was still only able to capture 39% of the variance again in part due to the large 2013 and 2015 events. Model equations and statistics are summarized in Table 4.

The *w*Q discharge metric was also able to predict mean annual SSI extent. A significant cubic relationship was observed between *w*Q and annual SSI ($y = 0.002x^3 + 0.09x^2 - 3.11x + 25.92$, $p < 0.001$, $R^2 = 0.71$; Fig. 10, bottom left panel). An exponential relationship was also identified between *w*Q and annual SSI ($y = 1.84 * 10^{0.047X}$, $p = 0.002$, $R^2 = 0.45$; Fig. 10, bottom right panel). The cubic model explains more of the variance in annual SSI extent than the exponential model (cubic $R^2 = 0.71$, exponential $R^2 = 0.45$). The cubic model is able to predict the two largest SSI extent events in 2011 and 2017 better than the exponential model which underestimates both years. The slightly negative trend in the cubic model from 5 to 10 *w*Q is likely unrealistic and simply an artifact of small extent variability in the lowest three observations. Model equations and statistics are summarized in Table 4.

Discussion

This study documents the development and validation of the first reported cyanoHAB monitoring product generated from the SeaWiFS sensor and the intercomparison with the MODIS cyanoHAB distribution product for Lake Erie. Modification of cyanoHAB/phytoplankton mapping algorithms for different remote sensing platforms and intercomparisons of their results is not new for Lake Erie. Wynne et al. (2013) modified the Cyanobacteria Index (CI) for application with

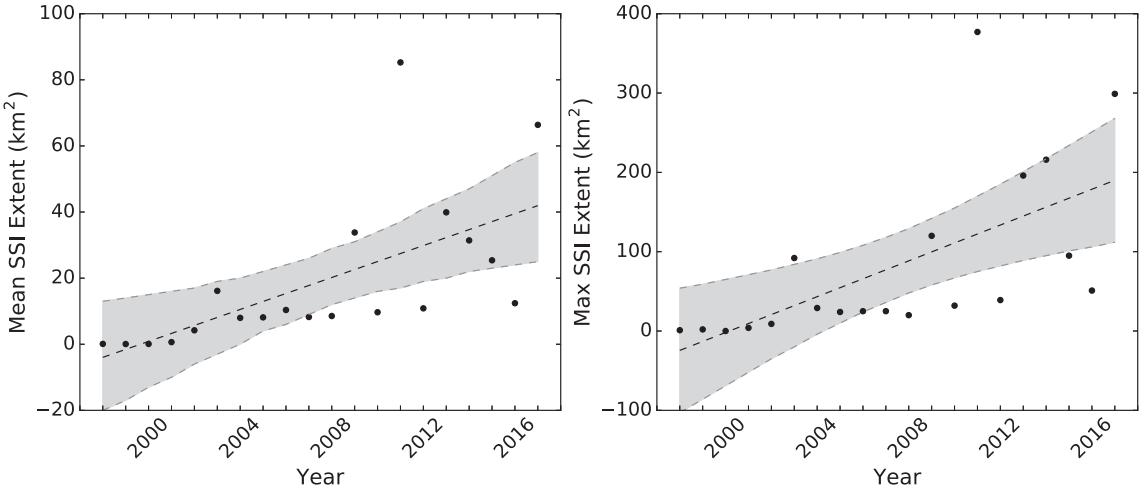

Fig. 6. (left panel) Annual mean scum extent (km^2) from the SSI with a linear best fit line (slope = 2.42, $R^2 = 0.39$, $p = 0.003$) and 95% confidence interval shaded in grey and (right panel) annual maximum scum extent with a linear best fit line (slope = 11.29, $R^2 = 0.39$, $p = 0.003$) and 95% confidence interval shaded in grey. Points from 1999 to 2001 come from the SeaWiFS sensor; points from 2002 to 2017 come from the MODIS Aqua sensor. The linear fits in the figure are not intended for scum area prediction.

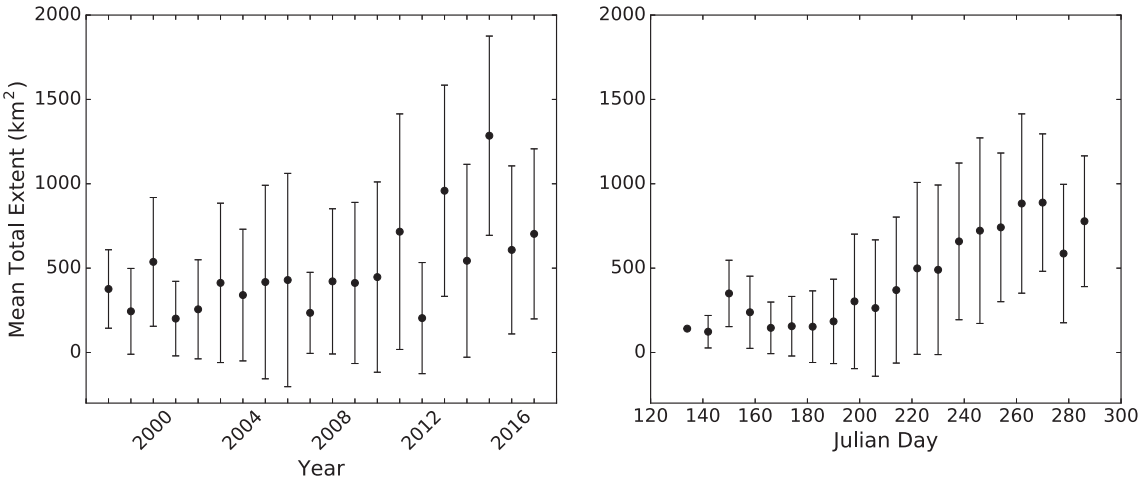

Fig. 7. left panel, Mean total cyanoHAB extent (floating and nonfloating) over the 20-year data record in Western Basin Lake Erie plotted with standard deviation errors. right panel, Mean 8-day seasonal pattern of total cyanoHAB extent in Western Basin Lake Erie, plotted with standard deviation error bars.

MODIS and showed generally good agreement between basin-wide cyanoHAB distributions. This modification allowed for a longer time-series (2002–2015) to be used to generate the NOAA cyanoHAB forecast model currently in operation (Stumpf et al., 2016). Similarly, Ho et al. (2017) evaluated multiple Landsat 5 algorithms to estimate phytoplankton blooms and compared the results with those obtained from the MERIS and MODIS CI products. The Landsat 5 inter-comparison allowed for a longer phytoplankton bloom time record (1984–2015) to be developed which was further used to explore the interaction of long-term internal loading of dissolved reactive phosphorus (DRP) and annual spring loadings to better predict phytoplankton blooms in western Lake Erie (Ho et al., 2017). While the Landsat data integration allows for a much longer time-series, the 16-day revisit time in conjunction with frequent cloud cover limit its ability to provide seasonal variability as well as robust uncertainties in annual extents. Prior to this study, SeaWiFS has not been used to map or monitor cyanoHAB presence in the Great Lakes. Other researchers have previously used SeaWiFS data to extend cyanoHAB observations in other water bodies throughout the world (Miller et al., 2006; Kahru et al., 2007; Kahru and Elmgren, 2014) to improve understanding of long-term environmental changes. Results from these studies indicated the added value of including SeaWiFS data in long-term monitoring of cyanoHAB distributions, strongly suggesting similar value would be expected from its application in Great Lakes water bodies. Incorporation of daily revisit SeaWiFS data into the time series extends the previously derived MODIS record (2002–2013; Sayers et al., 2016) back to 1998 providing more robust annual and seasonal observations to better understand how cyanoHAB dynamics have changed over the past 20 years. This new dataset clearly augments those cyanoHAB products previously developed for Lake Erie (Stumpf et al., 2012, 2016; Sayers et al., 2016; Ho et al., 2017).

The annual trends generated by the new SeaWiFS/MODIS integrated cyanoHAB extent products are similar to those produced by prior investigators that used the MERIS sensor which has been well documented to produce robust cyanoHAB estimates (Stumpf et al., 2012; Wynne et al., 2013). There are several differences in the methodologies that can lead to different results, however. The Cyanobacteria Index (CI) uses MERIS spectral bands located at 665, 681, and 709 nm to relate the spectral shape in this wavelength region to abundance of cyanobacteria (Gower et al., 1999; Wynne et al., 2008). In the case of high phytoplankton/cyanobacteria biomass, particulate scattering (possibly enhanced due to cyanobacteria cell structure) begins to overwhelm the signal from pure water absorption in the red edge spectral region forming a peak at ~709 nm while phycobilipigment fluorescence overwhelms chlorophyll-*a* absorption to form a peak around 665 nm (Matthews et al., 2012). These two peaks formed on both sides of the Q-band chlorophyll-*a* absorption feature (~675 nm) form a trough in reflectance at approximately 681 nm. The depth of this trough relative to the surrounding peaks is the basis for the CI estimation of cyanobacteria abundance. Because of the cyanobacteria particle scattering and phycobilipigment fluorescence dominance of this spectral response and the strong absorption by pure water, the CI requires a moderate presence of biomass before positive identification is achieved. For example, Rowe et al. (2016) related the CI low level of detection to approximately 23 mg/m^3 of chlorophyll-*a*. The MCH method used in this study is a full spectrum (412–667 nm) inversion model that takes into account both scattering and absorption processes to retrieve chlorophyll-*a* concentrations which are then empirically related to the cyanobacteria phycobilin pigment phycocyanin (Sayers et al., 2016). The MCH was shown to be able to empirically estimate phycocyanin when chlorophyll-*a* concentrations were >18 mg/m^3. Therefore, the difference between CI and MCH extent values may be related to the difference in each algorithm's low level of detection of chlorophyll-*a* biomass that in some cases can result in differences in the retrieved biomass/area of cyanoHAB blooms at very low concentrations that can be observed during the bloom initiation period.

Another unique aspect of this study is the generation of the cyanoHAB surface scum extent 20-year "heat map" which depicts areas experiencing intense blooms that have been associated with very high toxin levels making them a particularly high concern for public health (Bartram and Rees, 1999). Scums can form and dissipate rapidly with the shifts in prevailing wind and waves (Paerl and Ustach, 1982; Wynne et al., 2013; Rowe et al., 2016; Bosse et al., 2019 *this issue*) making them difficult to track and characterize with *in situ* measurements. The SSI approach used in this study makes use of the significant near-infrared scattering of surface algal mats to identify their presence from satellite sensors. Using the SSI to characterize scum occurrence for the 20-year time series identifies areas where scums are most often located. As expected, scums were common in the mouth of the Maumee River where very shallow waters, shelter from prevailing winds, and injection of critical nutrients occur. Significant scum occurrence was also identified around the islands with the most significant accumulations on the west ends that corresponds to the direction of the prevailing summer winds (from the southwest). These observations suggest scums can be formed as wind driven currents advect near-surface particles, which rapidly accumulate as they are pushed into the island shorelines. Underlying currents and surface winds may also be responsible for the observation that scum "hot spots" do not match those identified for the total cyanoHAB extent (cells mixed in the optical depth sampled from satellite remote sensing). For example, Bosse et al.

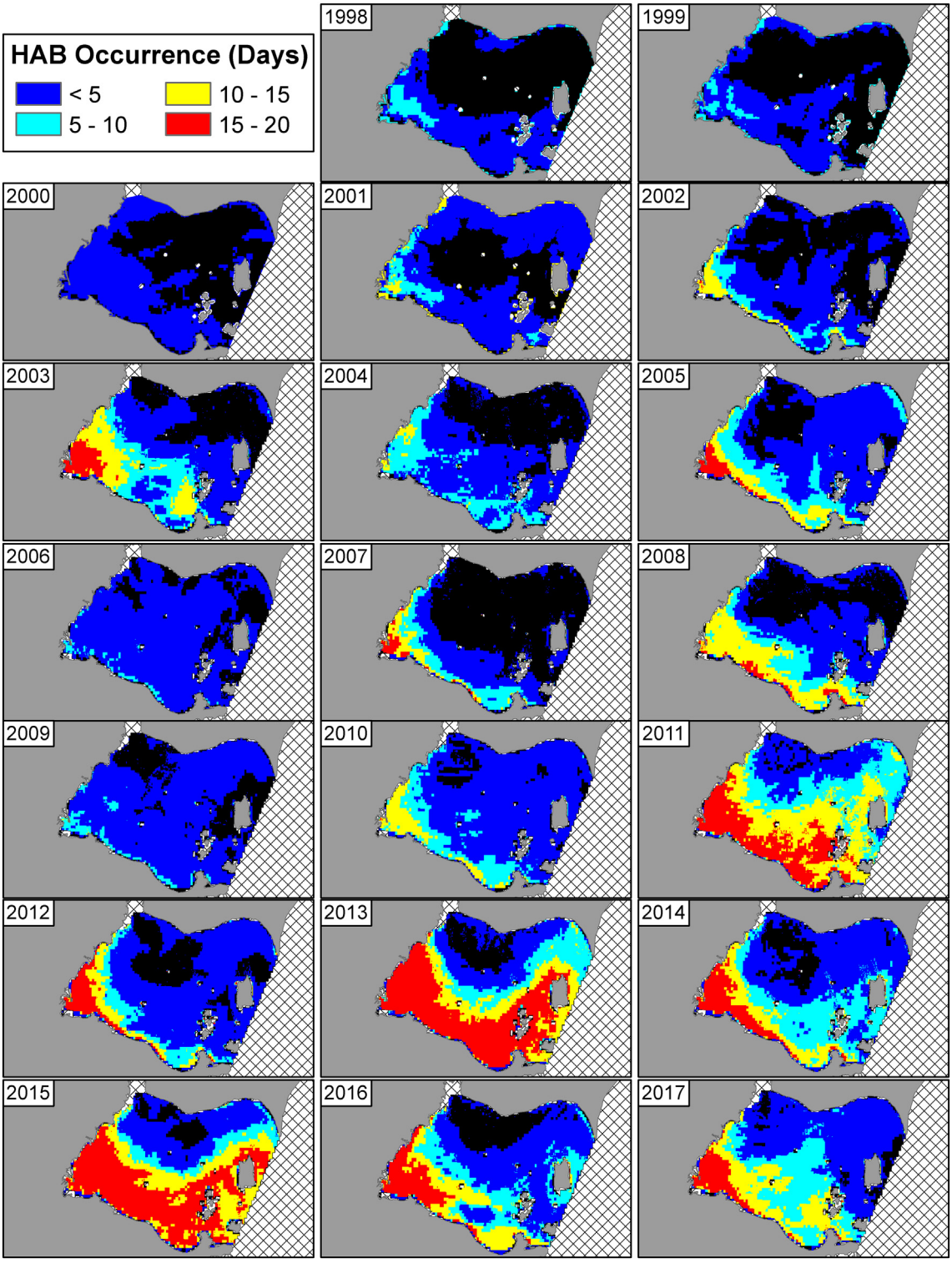

Fig. 8. Frequency of occurrence annual heat maps of cyanoHAB presence for the 1998–2017 period. Areas of more frequent occurrence are shown in warmer colors while areas of no-occurrence are shown in black. Data from 1999 to 2001 come from the SeaWiFS sensor; data from 2002 to 2017 come from the MODIS Aqua sensor.

(2019, this issue) suggested surface accumulations of high biomass cyanobacteria were more frequent in deeper waters under low wind conditions; whereas, shallower areas (<3 m) were more often well mixed under similar conditions. In this scenario, persistent high biomass blooms in shallow waters may often be well mixed which can be identified with the MCH but not SSI. This may be why the large shallow (2–6 m) area along the middle of the southern shoreline shows frequent blooms with MCH (Fig. 8) but essentially no scum occurrences (Fig. 9) over the 20-year period. Identification of scum "hot spots" is a new and unique aspect of this study that was previously unreported and will be particularly useful for regional water managers as well as for ecosystem modeling.

Annual cyanoHAB extents derived from the new 20-year integrated dataset reinforces the prevailing assumption that cyanoHABs are

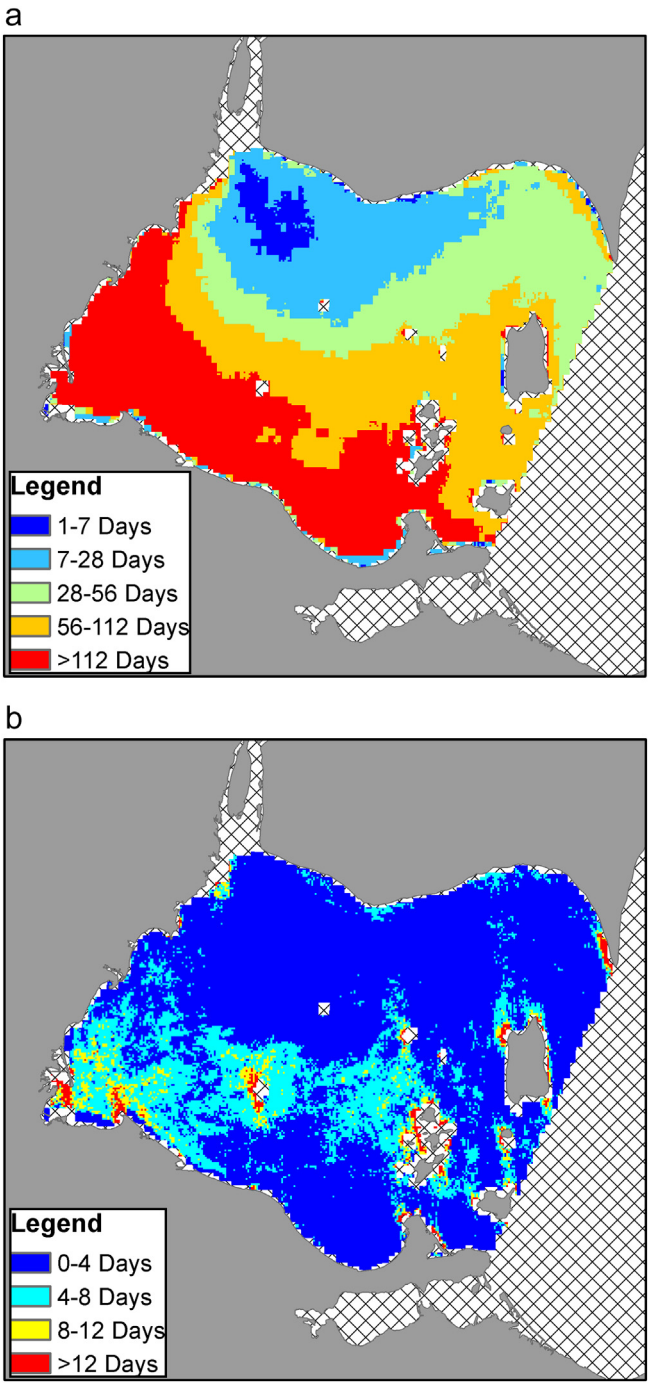

Fig. 9. Cumulative frequency of occurrence heat maps of total cyanoHABs (top) and surface scum (bottom) for the 1998–2017 period. Warmer colors indicate more frequent occurrence.

getting worse in Lake Erie. Multiple investigators have used remote sensing and *in situ* sampling data to determine that cyanoHAB extents are becoming larger and more prevalent in Lake Erie (Stumpf et al., 2012; Bridgeman et al., 2013; Michalak et al., 2013; Wynne and Stumpf, 2015; Sayers et al., 2016; Stumpf et al., 2016). For example, Stumpf et al. (2012), using MERIS data, showed maximum bloom areas were larger in 2008, 2009, and 2011 than previous years back to 2002. These observations were updated by Stumpf et al. (2016) using the merged MERIS and MODIS CI products which identified very large blooms in 2013 and 2015. Similarly, Sayers et al. (2016) also identified greater mean annual cyanoHAB extent in 2011 and 2013 for the western basin of Lake Erie. Finally, Bridgeman et al. (2013) noted from *in situ* observations that the 2011 bloom was 29 times larger than the smallest bloom recorded since 2002.

The addition of the 2016 and 2017 annual cyanoHAB extents presented in this study showed the continuation of the cyclical pattern in extents that began between 2010 and 2011. This pattern has been evident and increasing where, until 2017, every other year saw a new "all-time record" cyanoHAB extent. The down years between the peaks were also increasing at a relatively continuous rate, indicating even the so called "down" (relative to the previous year) cyanoHAB years (2012, 2014, 2016) are increasing in mean annual extent. Moreover, this study shows the substantial linear increase in maximum cyanoHAB extent throughout the time-series suggesting that even if the mean annual extent is not large there is a high probability of a very large bloom occurring for at least some period of time within each year moving forward. These results would agree with the conclusions of other researchers (Obenour et al., 2014; Matisoff et al., 2016; Watson et al., 2016; Ho and Michalak, 2017) that suggest other factors beyond spring phosphorus loading are driving the increase in blooms observed since 2010.

The new 20-year fused cyanoHAB time series allows for the evaluation or re-formation of predictive models in the face of changing environmental and meteorological drivers. While previous models have allowed for general predictions, our analysis suggests that much variability is still unaccounted for and future predictions based on these simple models need to be used with caution. Stumpf et al. (2012) reported the first cyanoHAB prediction model that established an exponential relationship between Maumee River spring discharge and CI-derived abundance from the 2002–2011 period. Sayers et al. (2016) found similar significant relationships between spring discharge and mean annual total and surface scum extents, respectively for the 2002–2013 period. This study found the 20-year time-series extent data to generally agree with the mean spring discharge models of Stumpf et al. (2012) and Sayers et al. (2016), but with greater deviations (and less predictive power) observed in larger outlier bloom years (2013 and 2015). This study also showed better prediction of extents using the *w*Q, the weighted discharge metric suggested by Stumpf et al. (2016); however, there was still a significant amount of unexplained variance suggesting that spring discharge alone is of limited prediction power for very large bloom extents. Stumpf et al. (2016) discusses the unique set of conditions, including bloom initiation location and high turbidity, which possibly resulted in the large outlier bloom in 2015 that was not well predicted by discharge alone. This observation is in agreement with the finding of Sayers et al. (2016) that the annual frequency of sediment re-suspension events have some power to predict large cyanoHAB blooms.

Observed variance in the weighted discharge, *w*Q, prediction of the 20-year time series data is also possible due to the inherent difference in modeled metrics of annual cyanoHABs. The NOAA operational forecast (Stumpf et al., 2016) is built upon a predictive model using discharge to estimate cyanoHAB biomass (summation of individual image pixel CI values) and not areal extent where the new 20-year time series data are estimates of areal extent regardless of biomass. The two metrics provide different information as there is the possibility to achieve a single basin-wide biomass value from either a spatially limited bloom of very high biomass or a large spatial bloom of low biomass. The new integrated SeaWiFS/MODIS extent products provide a complementary dataset (to the NOAA CI product) to approach annual cyanoHAB predictions.

Conclusions and recommendations

This new extended 20-year time series for the Western Basin of Lake Erie provides more quantitative support for the widespread observation that cyanoHABs have become more severe (larger and longer lasting) in recent years, beginning in the mid-2000s and accelerating after 2010. Comparison of the SeaWiFS and MODIS Aqua products at the pixel,

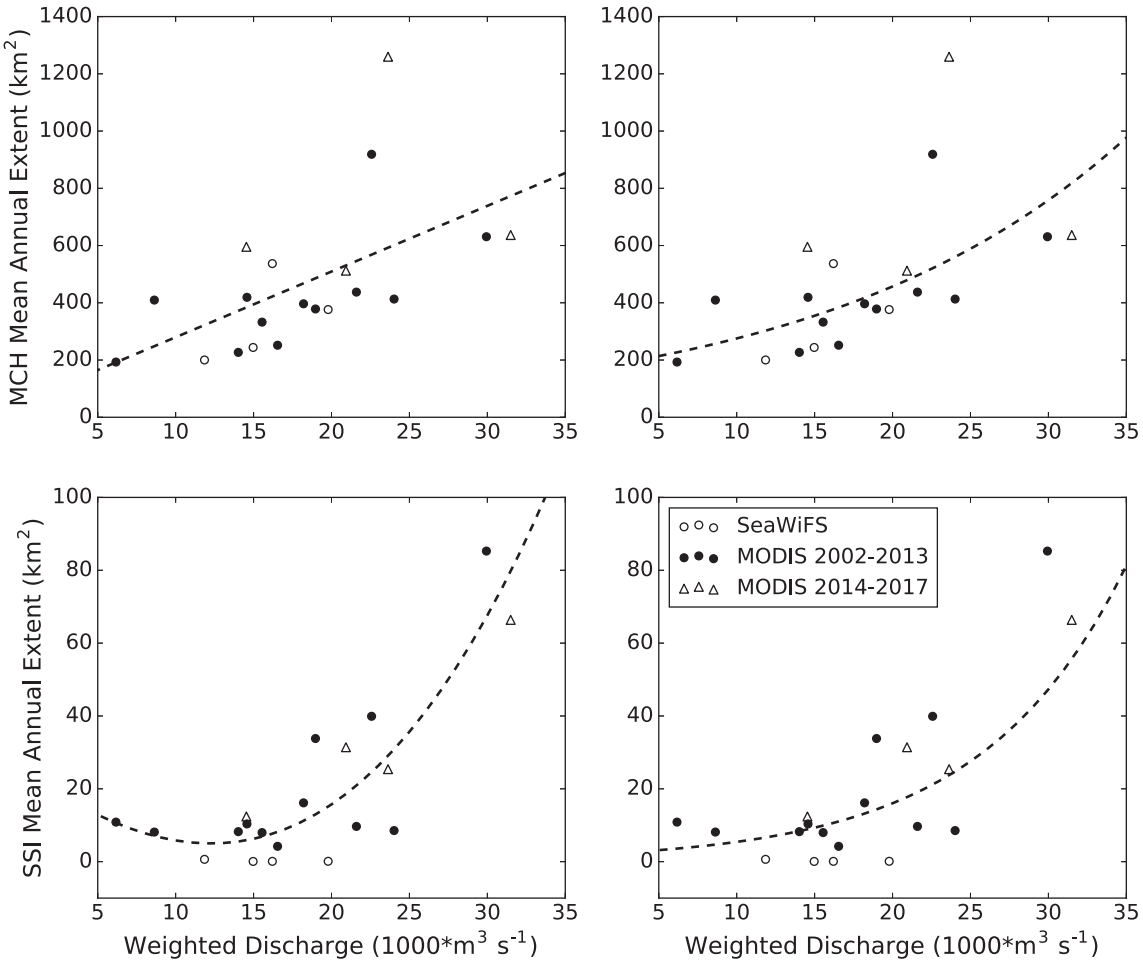

Fig. 10. Relationships between Maumee River weighted spring discharge, wQ, and (top left) MCH mean annual extent linear fit ($y = 1.53\times + 64.14$, $p = 0.01$, $R^2 = 0.27$), (top right) MCH mean annual extent exponential fit ($y = 165.92 * 10^{0.022x}$, $p = 0.002$, $R^2 = 0.39$), (bottom left) SSI mean annual extent cubic fit ($y = 0.002x^3 + 0.09x^2 - 3.11x + 25.92$, $p < 0.001$, $R^2 = 0.71$), and (bottom right) SSI mean annual extent exponential fit ($y = 1.84 * 10^{0.047x}$, $p = 0.002$, $R^2 = 0.45$). Plotted lines represent the best fits lines for each relationship. Open circles are the extents derived from SeaWiFS data, closed circles are from MODIS data reported in Sayers et al. (2016), and open triangles are from MODIS data reported in this study.

daily, and annual scales confirm that the imagery from these two sensors was successfully fused into a single, consistent time series. Including SeaWiFS imagery from years prior to the launch of MODIS Aqua demonstrated that these earlier cyanoHAB events were smaller than in later years but spatially similar, with the most persistent and intense blooms located in Maumee Bay and along the southern shore of the basin with very little activity in the Detroit River outflow. Looking at the cumulative occurrence map for the 20-year time series (Fig. 9), only the plume of Detroit River water in the northwest corner of WBLE has consistently remained cyanoHAB-free.

This 20-year time series demonstrates the complexity of relating cyanoHABs extent and duration to simple drivers such as river discharge. The 20-year record, which includes 8-day seasonal composites, can be used to further quantify the effect of other drivers including meteorological conditions, resuspension events, land cover changes, and agricultural practices on cyanoHABs extent and duration.

The MCH/SSI method could be further adapted for use with the CZCS imagery of Lake Erie collected from 1979 to 1987, providing better historical context for Lake Erie. This extends to the time period pre-mussel invasion and thus could allow for the quantification of the impact of these mussels on cyanoHAB events. The method could also be extended spatially, given that some Lake Erie cyanoHABs in recent years have extended into the central basin of the lake. Finally, the sediment plume maps incidentally produced as part of the MCH could be developed into their own time series to better understand variations in erosion and sediment load in the Maumee River.

Table 4
MCH and SSI extent model equations and statistics. Extent models are derived using the weighted spring discharge metric (*w*Q) as the predictor.

Model	Equation	R^2	p-Value
MCH linear	$1.53x + 64.14$	0.27	0.01
MCH exponential	$165.92 * 10^{0.022x}$	0.39	0.002
SSI cubic	$0.002x^3 + 0.09x^2 - 3.11x + 25.92$	0.71	<0.001
SSI exponential	$1.84 * 10^{0.047x}$	0.45	0.002

Acknowledgements

Generation of recent MODIS cyanoHAB products was funded by the US Environmental Protection Agency (EPA), NOAA GLERL, and CIGLR under subcontract #3004701270. Aspects of this study were also supported by the EPA under contract EP-R5-11-07 through subcontract #427998 from Battelle Memorial Institute. The study was based on previous work supported by the EPA under grant GL-00E00855-0 as well as by the Great Lakes Observing System under contract #3002475304 and The University of Michigan Water Center under contract #3003032930. Aspects of this study were funded by the NASA Carbon Monitoring System under contract #80NSSC17K0712. We thank Harry Stone and

Stephanie Weber at Battelle for their technical feedback and review of the work on which this study was based. We would also like to acknowledge Beth Hinchey-Malloy and Frank Anscombe from EPA GLNPO for their technical contributions and encouragement.

References

Abbott, M.R., Letelier, R.M., 1999. Algorithm Theoretical Basis Document Chlorophyll Fluorescence (MODIS Product Number 20). NASA http://www.modis.gsfc.nasa.gov/data/atbd.

Ali, K., Witter, D., Ortiz, J., 2014. Application of empirical and semi-analytical algorithms to MERIS data for estimating chlorophyll a in case 2 waters of Lake Erie. Environ. Earth Sci. 71 (9), 4209–4220.

Bartram, J., Rees, G. (Eds.), 1999. Monitoring Bathing Waters: A Practical Guide to the Design and Implementation of Assessments and Monitoring Programmes. CRC Press.

Becker, R.H., Sultan, M.I., Boyer, G.L., Twiss, M.R., Konopko, E., 2009. Mapping cyanobacterial blooms in the Great Lakes using MODIS. J. Great Lakes Res. 35 (3), 447–453.

Bosse, K.R., Sayers, M.J., Shuchman, R.A., Fahnenstiel, G.L., Ruberg, S.A., Fanslow, D.L., Stuart, D.G., Johengen, T.H., Burtner, A.M., 2019. Spatial-temporal variability of cyanobacteria vertical structure in Western Lake Erie: implications for remote sensing observations. J. Great Lakes Res. (this issue).

Bridgeman, T.B., Chaffin, J.D., Filbrun, J.E., 2013. A novel method for tracking western Lake Erie Microcystis blooms, 2002–2011. J. Great Lakes Res. 39 (1), 83–89.

Budd, J.W., Warrington, D.S., 2004. Satellite-based sediment and chlorophyll a estimates for Lake Superior. J. Great Lakes Res. 30, 459–466.

Budd, J.W., Beeton, A.M., Stumpf, R.P., Culver, D.A., Charles Kerfoot, W., 2001. Satellite observations of *Microcystis* blooms in western Lake Erie. Verh. Int. Ver. Theor. Angew. Limnol. 27 (7), 3787–3793.

Bukata, R.P., Jerome, J.H., Kondratyev, A.S., Pozdnyakov, D.V., 1995. Optical Properties and Remote Sensing of Coastal and Inland Waters. CRC Press.

Cullen, J.J., Ciotti, A.M., Davis, R.F., Lewis, M.R., 1997. Optical detection and assessment of algal blooms. Limnol. Oceanogr. 42 (5part2), 1223–1239.

Dash, P., Walker, N., Mishra E., D'Sa, Ladner, S., 2012. Atmospheric correction and vicarious calibration of Oceansat-1 Ocean Color Monitor (OCM) data in coastal case 2 waters. Remote Sens. 4 (6), 1716–1740.

Dekker, A.G., 1993. Detection of Optical Water Quality Parameters for Eutrophic Waters by High Resolution Remote Sensing.

Duan, H., Ma, R., Xu, X., Kong, F., Zhang, S., Kong, W., Hao, J., Shang, L., 2009. Two-decade reconstruction of algal blooms in China's Lake Taihu. Environ. Sci. Technol. 43 (10), 3522–3528.

Duan, H., Ma, R., Simis, S.G., Zhang, Y., 2012. Validation of MERIS case-2 water products in Lake Taihu, China. GIScience Remote Sens. 49 (6), 873–894.

Dupouy, C., Petit, M., Dandonneau, Y., 1988. Satellite detected cyanobacteria bloom in the southwestern tropical Pacific implication for oceanic nitrogen fixation. Remote Sens. 9 (3), 389–396.

Gons, H.J., 1999. Optical teledetection of chlorophyll a in turbid inland waters. Environ. Sci. Technol. 33 (7), 1127–1132.

Gower, J.F.R., Doerffer, R., Borstad, G.A., 1999. Interpretation of the 685 nm peak in water-leaving radiance spectra in terms of fluorescence, absorption and scattering, and its observation by MERIS. Int. J. Remote Sens. 20 (9), 1771–1786.

Hawley, N., Johengen, T.H., Rao, Y.R., Ruberg, S.A., Beletsky, D., Ludsin, S.A., Eadie, B.J., Schwab, D.J., Croley, T.E., Brandt, S.B., 2006. Lake Erie hypoxia prompts Canada-US study. Eos. Trans. AGU 87 (32), 313–319.

Ho, J.C., Michalak, A.M., 2015. Challenges in tracking harmful algal blooms: a synthesis of evidence from Lake Erie. J. Great Lakes Res. 41 (2), 317–325.

Ho, J.C., Michalak, A.M., 2017. Phytoplakton blooms in Lake Erie impacted by both long-term and springtime phosphorus loading. J. Great Lakes Res. 43 (3), 221–228.

Ho, J.C., Stumpf, R.P., Bridgeman, T.B., Michalak, A.M., 2017. Using Landsat to extend the historical record of lacustrine phytoplankton blooms: a Lake Erie case study. Remote Sens. Environ. 191, 273–285.

Hu, C., 2009. A novel ocean color index to detect floating algae in the global oceans. Remote Sens. Environ. 113 (10), 2118–2129.

Hu, C., Lee, Z., Ma, R., Yu, K., Li, D., Shang, S., 2010. Moderate resolution imaging spectroradiometer (MODIS) observations of cyanobacteria blooms in Taihu Lake, China. J. Geophys. Res. Oceans 115 (C4).

Huang, C., Li, Y., Yang, H., Sun, D., Yu, Z., Zhang, Z., Chen, X., Xu, L., 2014. Detection of algal bloom and factors influencing its formation in Taihu Lake from 2000 to 2011 by MODIS. Environ. Earth Sci. 71 (8), 3705–3714.

IOCCG, 2007. Ocean Colour Data Merging. In: Gregg, W.W. (Ed.), Reports of the International Ocean-Colour Coordinating Group. 5. IOCCG, Dartmouth, Canada, p. 65.

Jerlov, N.G., 1976. Marine Optics. Vol. 14. Elsevier.

Ju, J., Roy, D.P., 2008. The availability of cloud-free Landsat ETM+ data over the conterminous United States and globally. Remote Sens. Environ. 112 (3), 1196–1211.

Kahru, M., Elmgren, R., 2014. Multidecadal time series of satellite-detected accumulations of cyanobacteria in the Baltic Sea. Biogeosciences 11 (13), 3619.

Kahru, M., Leppanen, J.M., Rud, O., 1993. Cyanobacterial blooms cause heating of the sea surface. Mar. Ecol. Prog. Ser. 1–7.

Kahru, M., 1997. Using satellites to monitor large-scale environmental change: a case study of cyanobacteria blooms in the Baltic Sea. Monitoring algal blooms: new techniques for detecting large-scale environmental change. Springer, Berlin, pp. 43–61.

Kahru, M., Leppänen, J.M., Rud, O., Savchuk, O.P., 2000. Cyanobacteria blooms in the Gulf of Finland triggered by saltwater inflow into the Baltic Sea. Mar. Ecol. Prog. Ser. 207, 13–18.

Kahru, M., Savchuk, O.P., Elmgren, R., 2007. Satellite measurements of cyanobacterial bloom frequency in the Baltic Sea: interannual and spatial variability. Mar. Ecol. Prog. Ser. 343, 15–23.

Kutser, T., 2004. Quantitative detection of chlorophyll in cyanobacterial blooms by satellite remote sensing. Limnol. Oceanogr. 49 (6), 2179–2189.

Lekki, J., Deutsch, E., Sayers, M., Bosse, K., Anderson, R., Tokars, R., 2019. Determining remote sensing spatial resolution requirements for the monitoring of harmful algal blooms in the Great Lakes. J. Great Lakes Res. (this issue).

Li, L., Li, L., Song, K., Li, Y., Tedesco, L.P., Shi, K., Li, Z., 2013. An inversion model for deriving inherent optical properties of inland waters: establishment, validation and application. Remote Sens. Environ. 135, 150–166.

Li, L., Li, L., Song, K., 2015. Remote sensing of freshwater cyanobacteria: an extended IOP inversion model of inland waters (IIMIW) for partitioning absorption coefficient and estimating phycocyanin. Remote Sens. Environ. 157, 9–23.

Matisoff, G., Kaltenberg, E.M., Steely, R.L., Hummel, S.K., Seo, J., Gibbons, K.J., Bridgeman, T.B., Seo, Y., Behbahani, M., James, W.F., Johnson, L.T., Doan, P., Dittrich, M., Evans, M.A., Chaffin, J.D., 2016. Internal loading of phosphorus in western Lake Erie. J. Great Lakes Res. 42 (4), 775–788.

Matthews, M.W., 2014. Eutrophication and cyanobacterial blooms in South African inland waters: 10 years of MERIS observations. Remote Sens. Environ. 155, 161–177.

Matthews, M.W., Bernard, S., 2015. Eutrophication and cyanobacteria in South Africa's standing water bodies: a view from space. S. Afr. J. Sci. 111 (5–6), 1–8.

Matthews, M.W., Bernard, S., Winter, K., 2010. Remote sensing of cyanobacteria-dominant algal blooms and water quality parameters in Zeekoevlei, a small hypertrophic lake, using MERIS. Remote Sens. Environ. 114 (9), 2070–2087.

Matthews, M.W., Bernard, S., Robertson, L., 2012. An algorithm for detecting trophic status (chlorophyll-*a*), cyanobacterial-dominance, surface scums and floating vegetation in inland and coastal waters. Remote Sens. Environ. 124, 637–652.

Michalak, A.M., Anderson, E., Beletsky, D., Boland, S., Bosch, N.S., Bridgeman, T.B., Chaffin, J.D., Cho, K.H., Confesor, R., Daloğlu, I., DePinto, J., Evans, M.A., Fahnenstiel, G.L., He, L., Ho, J.C., Jenkins, L., Johengen, T., Kuo, K.C., Laporte, E., Liu, X., McWilliams, M., Moore, M.R., Posselt, D.J., Richards, R.P., Scavia, D., Steiner, A.L., Verhamme, E., Wright, D.M., Zagorski, M.A., 2013. Record-setting algal bloom in Lake Erie caused by agricultural and meteorological trends consistent with expected future conditions. Proc. Natl. Acad. Sci. 110 (16), 6448–6452.

Miller, P.I., Shutler, J.D., Moore, G.F., Groom, S.B., 2006. SeaWiFS discrimination of harmful algal bloom evolution. Int. J. Remote Sens. 27 (11), 2287–2301.

Mishra, S., Mishra, D.R., 2012. Normalized difference chlorophyll index: a novel model for remote estimation of chlorophyll-*a* concentration in turbid productive waters. Remote Sens. Environ. 117, 394–406.

Mishra, D.R., Ogashawara, I., Gitelson, A.A., 2017. Bio-optical Modeling and Remote Sensing of Inland Waters. Elsevier.

Obenour, D.R., Gronewold, A.D., Stow, C.A., Scavia, D., 2014. Using a Bayesian hierarchical model to improve Lake Erie cyanobacteria bloom forecasts. Water Resour. Res. 50 (10), 7847–7860.

Oberholster, P.J., Botha, A.M., 2010. Use of remote sensing and molecular markers to detect toxic cyanobacterial hyperscum crust: a case study on Lake Hartbeespoort, South Africa. Afr. J. Biotechnol. 9 (51), 8791–8799.

Paerl, H.W., Ustach, J.F., 1982. Blue-green algal scums: an explanation for their occurrence during freshwater blooms. Limnol. Oceanogr. 27 (2), 212–217.

Peng, W.X., Wang, H.Y., Jiang, Q.W., 2008. Dynamic change monitoring of cyanobacterial blooms using multi-temporal satel lite data in Lake Taihu. Fudan Univ. J. Med. Sci. 35 (1), 63.

Pettersson, L.H., Pozdnyakov, D., 2012. Monitoring of Harmful Algal Blooms. Springer Science & Business Media.

Reinart, A., Kutser, T., 2006. Comparison of different satellite sensors in detecting cyanobacterial bloom events in the Baltic Sea. Remote Sens. Environ. 102 (1–2), 74–85.

Rinta-Kanto, J.M., Ouellette, A.J.A., Boyer, G.L., Twiss, M.R., Bridgeman, T.B., Wilhelm, S.W., 2005. Quantification of toxic *Microcystis* spp. during the 2003 and 2004 blooms in western Lake Erie using quantitative real-time PCR. Environ. Sci. Technol. 39 (11), 4198–4205.

Rowe, M.D., Anderson, E.J., Wynne, T.T., Stumpf, R.P., Fanslow, D.L., Kijanka, K., Vanderploeg, H.A., Strickler, J.R., Davis, T.W., 2016. Vertical distribution of buoyant Microcystis blooms in a Lagrangian particle tracking model for short-term forecasts in Lake Erie. J. Geophys. Res. Oceans 121 (7), 5296–5314.

Sayers, M., Fahnenstiel, G.L., Shuchman, R.A., Whitley, M., 2016. Cyanobacteria blooms in three eutrophic basins of the Great Lakes: a comparative analysis using satellite remote sensing. Int. J. Remote Sens. 37 (17), 4148–4171.

Schalles, J.F., Yacobi, Y.Z., 2000. Remote detection and seasonal patterns of phycocyanin, carotenoid and chlorophyll pigments in eutrophic waters. Ergeb. Limnol. 55, 153–168.

Schwab, D.J., Leshkevich, G.A., Muhr, G.C., 1999. Automated mapping of surface water temperature in the Great Lakes. J. Great Lakes Res. 25 (3), 468–481.

Shuchman, R., Korosov, A., Hatt, C., Pozdnyakov, D., Means, J., Meadows, G., 2006. Verification and application of a bio-optical algorithm for Lake Michigan using SeaWiFS: a 7-year inter-annual analysis. J. Great Lakes Res. 32 (2), 258–279.

Shuchman, R.A., Leshkevich, G., Sayers, M.J., Johengen, T.H., Brooks, C.N., Pozdnyakov, D., 2013. An algorithm to retrieve chlorophyll, dissolved organic carbon, and suspended minerals from Great Lakes satellite data. J. Great Lakes Res. 39, 14–33.

Simis, S.G., Peters, S.W., Gons, H.J., 2005. Remote sensing of the cyanobacterial pigment phycocyanin in turbid inland water. Limnol. Oceanogr. 50 (1), 237–245.

Simis, S.G., Ruiz-Verdú, A., Domínguez-Gómez, J.A., Peña-Martinez, R., Peters, S.W., Gons, H.J., 2007. Influence of phytoplankton pigment composition on remote sensing of cyanobacterial biomass. Remote Sens. Environ. 106 (4), 414–427.

Steffen, M.M., Belisle, B.S., Watson, S.B., Boyer, G.L., Wilhelm, S.W., 2014. Status, causes and controls of cyanobacterial blooms in Lake Erie. J. Great Lakes Res. 40 (2), 215–225.

Stumpf, R.P., Wynne, T.T., Baker, D.B., Fahnenstiel, G.L., 2012. Interannual variability of cyanobacterial blooms in Lake Erie. PLoS One 7 (8), e42444.
Stumpf, R.P., Johnson, L.T., Wynne, T.T., Baker, D.B., 2016. Forecasting annual cyanobacterial bloom biomass to inform management decisions in Lake Erie. J. Great Lakes Res. 42 (6), 1174–1183.
Ulbricht, K.A., 1983. Cover photograph LANDSAT image of blue green algae in the Baltic sea. Int. J. Remote Sens. 4 (4), 801–802.
Vanderploeg, H.A., Liebig, J.R., Carmichael, W.W., Agy, M.A., Johengen, T.H., Fahnenstiel, G.L., Nalepa, T.F., 2001. Zebra mussel (*Dreissena polymorpha*) selective filtration promoted toxic Microcystis blooms in Saginaw Bay (Lake Huron) and Lake Erie. Can. J. Fish. Aquat. Sci. 58 (6), 1208–1221.
Vincent, R.K., Qin, X., McKay, R.M.L., Miner, J., Czajkowski, K., Savino, J., Bridgeman, T., 2004. Phycocyanin detection from LANDSAT TM data for mapping cyanobacterial blooms in Lake Erie. Remote Sens. Environ. 89 (3), 381–392.
Watson, S.B., Miller, C., Arhonditsis, G., Boyer, G.L., Carmichael, W., Charlton, M.N., Confesor, R., Depew, D.C., Höök, T.O., Ludsin, S.A., Matisoff, G., MeElmurry, S.P., Murray, M.W., Richards, R.P., Rao, Y.R., Steffen, M.M., Wilhelm, S.W., 2016. The re-eutrophication of Lake Erie: harmful algal blooms and hypoxia. Harmful Algae 56, 44–66.
Witter, D.L., Ortiz, J.D., Palm, S., Heath, R.T., Budd, J.W., 2009. Assessing the application of SeaWiFS ocean color algorithms to Lake Erie. J. Great Lakes Res. 35 (3), 361–370.
Wynne, T.T., Stumpf, R.P., 2015. Spatial and temporal patterns in the seasonal distribution of toxic cyanobacteria in Western Lake Erie from 2002–2014. Toxins 7 (5), 1649–1663.
Wynne, T.T., Stumpf, R.P., Tomlinson, M.C., Warner, R.A., Tester, P.A., Dyble, J., Fahnenstiel, G.L., 2008. Relating spectral shape to cyanobacterial blooms in the Laurentian Great Lakes. Int. J. Remote Sens. 29 (12), 3665–3672.
Wynne, T.T., Stumpf, R.P., Tomlinson, M.C., Dyble, J., 2010. Characterizing a cyanobacterial bloom in western Lake Erie using satellite imagery and meteorological data. Limnol. Oceanogr. 55 (5), 2025–2036.
Wynne, T.T., Stumpf, R.P., Briggs, T.O., 2013. Comparing MODIS and MERIS spectral shapes for cyanobacterial bloom detection. Int. J. Remote Sens. 34 (19), 6668–6678.